Chemical Physics Letters 706 (2018) 708–714

Contents lists available at ScienceDirect

Chemical Physics Letters

journal homepage: www.elsevier.com/locate/cplett

Research paper

Insight into mechanism of iron-oxides reduction in atmospheres of CH_4 and CO

Tetiana Zubatiuk [a,*], Glake Hill [a], Danuta Leszczynska [a], Maohong Fan [b], Asif H. Rony [b], Jerzy Leszczynski [a]

[a] Interdisciplinary Center for Nanotoxicity, Jackson State University, 1400 J. R. Lynch Street, Jackson, MS 39217, USA
[b] Departments of Chemical and Petroleum Engineering, University of Wyoming, Laramie, WY 82071, USA

ARTICLE INFO

Article history:
Received 11 May 2018
In final form 12 July 2018

Keywords:
Iron oxide
Carburization
CO conversion
CH_4 conversion
DFT
IRC
NBO

ABSTRACT

First-principle calculations are carried out to interpret the experimental observations and to generate the mechanisms of CO and CH_4 conversion with Fe_2O_{1-3}. The stabilization of Fe—C bonding involves π^*(C—O) and electron donating from oxygens' LP. The Fe—O bond activation is rate-limiting step of conversions. Stabilization and activation are affected by number of oxygens at the iron active site. Low ORBs are identified for CO + Fe_2O_{1-3} reaction pathways. Significant ORBs are calculated for Fe_2O_3 + CH_4, and the competing mechanism of reduction by H_2 is shown. DFT calculations suggest favorable formation of Fe_3C in atmosphere of CH_4 and its oxidation in atmosphere of CO.

1. Introduction

Oxy-iron compounds (OIC) are known to be an important group of industrial heterogeneous catalysts [1]. The reactivity of OIC clusters toward various gas-phase molecules has been extensively investigated experimentally with emphasis on rate limiting steps in practical catalytic cycles. More can be found in Schroder et al. [2] review. However, molecular-level mechanisms of some processes catalyzed by OICs and the possible side-reactions are unclear. Recently, Ca—Fe based catalysts attracted an interest due to their potential in chemical looping hydrogen generation (CLHG) process [3,4]. Sun et al. [3] have shown that higher yields of hydrogen could be generated by using a novel Ca—Fe based oxygen carriers, which is proved to be a more stable formation of the calcium ferrite compounds and promising catalysts for CLHG process which show perfect reducibility, oxidation activity, and cyclic stability. Several types of compounds are known to participate in the Ca—Fe based catalysts [5]. In the Fe^{3+}-containing system of CaO–Fe_2O_3, the calcium ferrites with different molecular ratios are known: 2CaO–Fe_2O_3, CaO–Fe_2O_3 and CaO–2Fe_2O_3. The Fe^{n+}-containing systems of CaO–Fe_xO_y usually exhibiting a layered structure containing $3d^6$ iron atom in a high- and low spin distorted squareplanar coordination. This structure complicates the modeling and theoretical study of their catalytic activity and side-effects. For instance, the 2:1 compound, $Ca_2Fe_2O_5$, which is considered as an oxygen-deficient perovskite of the Brownmillerite-type of structure, exhibits the alternating tetrahedral and octahedral layers [5]. However, in spite of specific role of the incorporated alkaline earth metals (Mg, Ca, Be, Sr, Ba, Ra) in the ferrites catalysts, the basic concept is that a catalytic reaction occurs at specific catalytically active sites of iron [6,7]. That is why, we suppose that small gas-phase iron oxide clusters (neutral) composed of limited numbers of iron atoms could serve a good model system to investigate the intrinsic reaction mechanisms in OIC.

In this study we investigate the reactivity of iron oxide clusters (Fe_xO_y) toward CH_4 and CO and the possible carburization of iron active sites. The iron active site (Fe^*) is reduced and regenerated by the following general reactions:

(a) CO conversion:

$$Fe^* - O + CO \rightleftharpoons Fe^* + CO_2 \quad (R1)$$

$$Fe^* + H_2O \rightleftharpoons Fe^* - O + H_2 \quad (R1)$$

(b) CH_4 conversion:

$$Fe^* - O + CH_4 \rightleftharpoons Fe^* + CO + 2H_2; \quad (R2)$$

* Corresponding author.
E-mail address: tetiana.zubatiuk@icnanotox.org (T. Zubatiuk).

https://doi.org/10.1016/j.cplett.2018.07.027
0009-2614/

$$Fe^{*} + 0.5O_2 \rightleftharpoons Fe^{*} - O \quad (R2)$$

The mentioned above reduction experiments [3] revealed that oxygen carriers oxidize significantly smaller amount of CH_4 species compared to CO. Additionally, a weight increase has been observed from both CO and CH_4 conversions when the oxygen carrier was about to be completely reduced or was completely reduced. Frequently, in processes where gas mixtures containing CO or hydrocarbons, (such as methane and other gases) contact with the OIC at high temperature the problems with carburization can occur. According to the general reactions of carburization (R3, R4), the Fe_3C should form in presence of both, CO and CH_4. Meanwhile, in Fan et al. [3] experiments XRD analysis of final products revealed that all the CO reduced Ca—Fe based oxygen carriers existed in the form of CaO and Fe and none of the Fe_3C. At the same time, in atmosphere of methane, Fe_3C began to gradually accumulate. The possible reactions of carburization with different reducing agents are the following:

$$3Fe_2O_3 + 13CO \rightarrow 2Fe_3C + 11CO_2 \quad (R3)$$

$$3Fe_2O_3 + 2CH_4 + 5H_2 \rightarrow 2Fe_3C + 9H_2O \quad (R4)$$

In spite of importance of developing of sufficient technologies of CO and CH_4 oxidation, there exists a certain lack of comprehensive and systematic studies of the intrinsic reaction mechanism. This includes details how CO and CH_4 oxidation are catalyzed at a molecular level and what is a nature of side reactions. Various proposed mechanism arises according this issue. Li et al. concluded that the small particle size and the FeOOH component of their Fe_2O_3 catalyst contribute to the high catalytic performance [8]. Zheng et al. concluded that the high density of Fe atoms on the exposed {1 1 0} planes of their quasicubic R-Fe_2O_3 nanoparticles leads to the excellent catalytic reactivity [9]. Xue et al. observed significant reaction barriers for the reactions of Fe_2O_{4-5} with CO. The rate-limiting steps for this processes involve the O—O activation [10]. Huang et al. [11] explored processes of methane dissociation, on a-Fe_2O_3 (0 0 1) surface and found that sequential dissociations of CH_4 have the highest barriers. The formed H atoms may recombine to produce H_2 with significant activation barrier of at least 1.37 eV. In addition, they concluded that the CO production is more favorable than CO_2. First principle calculations were also used by Reddy and co-workers to study CO oxidation catalyzed by a neutral Fe_2O_3 cluster [12]. CO adsorption onto gas-phase Fe_2O_3 clusters causes rearrangement of one of the three Fe—O—Fe bridged bonds to one Fe—O terminal bond. A reaction barrier of 0.39 eV was calculated for CO approaching the Fe_2O_3 cluster. The Fe—O terminal bond can further oxidize another CO molecule to form CO_2 easily. The gas-phase experimental study by Xue et al. [10] for the neutral clusters later support those theoretical results.

In current study, the first-principle calculations (DFT) are used to explain the reactivity of OIC toward CO and CH_4 and to elucidate the results of experimental studies of Fan and co-workers [3,13]. The Fe_xO_y clusters have been used as the model of active sites. The details of the reaction mechanism are obtained and used to interpret at a molecular level catalytic process of CO and CH_4 oxidation by oxygen of OIC and the side-reaction mechanism of Fe_3C formation. The lattice oxygen of oxygen carrier, which involves in the real CLHG reactions is not under consideration in current study.

2. Computational methods

The quantum chemical calculations using the Gaussian 09 program [14] have been employed to study the multicycles of CO and CH_4 reduction on the Fe_2O, Fe_2O_2 and Fe_2O_3 clusters. Because of the lack in experimental data for neutral Fe_xO_y clusters, the spin state of Fe_2O_{1-3} model clusters was defined through the test of different C_{2v} Fe_2O_{1-3} conformers with different spin multiplicities. The conformers with the lowest electronic energy were chosen for further calculations. The spin conversion which is known to be important in many reaction systems involving transition metals [10,15] has not be employed in current study and is the subject of further investigations. Thus, we assume that the spin of the molecules preserves along the course of reaction. The reaction pathways are studied for $Fe_2O_{1-3} + CO \rightarrow Fe_2O_{1-2} + CO_2$, and $Fe_2O_{1-3} + H_2 \rightarrow Fe_2O_{1-2} + H_2O$. Additional pathways are followed for $Fe_2O_3 + CH_4 \rightarrow F_2O_2 + CO + 2H_2$, and $Fe_3C + CO_2 \rightarrow 3Fe + 2CO$. The reaction pathway calculations involve geometry optimizations of various reaction intermediates and transition states through which the intermediates transfer to each other. The transition state optimizations are performed by employing the either Berny algorithm [16] or the synchronous transit-guided quasi Newton (STQN) method [17]. Vibrational frequency calculations are performed to check that reaction intermediates and transition state species have zero and one imaginary frequencies, respectively. The hybrid ωB97XD exchange-correlation functional [18] which includes empirical dispersion is used. The basis set adopted is the balanced polarized triple-zeta def2tzvp basis set [19]. We believe, that the used long-range-corrected hybrid functional, ωB97XD accounts for the strongly correlated d-electrons of iron-oxide clusters, because it is shown to perform well in the comprehensive thermochemical benchmark set of metal organic reactions [20]. The studied reaction pathways are presented in the form of energy diagrams. Cartesian coordinates and energies ($E_{elec.}$, $H_{0\ K}$, $H_{298\ K}$, and $G_{298\ K}$) for all of the optimized structures (intermediates and transition states) are listed as Tables S1–4 in the Supporting Information. The relative free energies of the adducts and intermediates, shown on the diagrams were calculated under standard conditions (298.15 K, 1 atm) and represent the standard free energy change of the corresponding reaction, as $\Delta G^0(rxn) = \sum \Delta G_f^0(products) - \sum \Delta G_f^0(reactants)$.

Supplementary data associated with this article can be found, in the online version, at https://doi.org/10.1016/j.cplett.2018.07.027.

3. Computational results

To test the validity of the ωB97XD/def2tzvp method for calculation of reaction pathways for multicycles of CO and CH_4 oxidation by Fe_xO_y, the bond dissociation energies (D°) and the bond lengths (r_e), are calculated and compared with experimental values for CO, CH_4, and FeO molecules. We used set of pure generalized gradient approximation functionals, GGA (BP86 [21] and PBE [22]), meta-GGA functional (TPSS [23]) and dispersion corrected range separated hybrid functional (ωB97XD [18]). The bond dissociation energy D° for a bond A-B which is broken through the reaction AB → A + B is defined here as the standard-state enthalpy change for the reaction at a 298.15 K. That is, $D^\circ = \Delta Hf^\circ_0(A) + \Delta Hf^\circ_0(B) - \Delta Hf^\circ_0(AB)$, where ΔHf°_0 is the standard-state heat of formation. The comparison is given in Table 1.

The ωB97XD functional shows excellent performance for bond length (within 0.02 Å) calculations. This functional little underestimates D° of CO and CH_4 by 0.19 and 0.12 eV, respectively. The D° value of FeO calculated through the ωB97XD functional is greater than experimental value by 0.09 eV. That is expected since in the simplest case where the bond of a diatomic molecule is broken, D° at 298 K is greater than D° at 0 K by an amount which lies between RT and (3/2) RT (i.e. 0.03–0.04 eV). We expect that the relative energetics for multicycles of CO and CH_4 oxidation by Fe_xO_y, can be reasonably predicted by ωB97XD/def2tzvp since the calculated D° value of FeO is accurate enough. The BP86 functional, which has a good performance for electron affinity calculations, overestimates D° values, and the largest error (>1 eV) occurs for

Table 1
Comparison of DFT/def2tzvp calculated at 298 K and experimental bond length (r_e in 0.1 nm) and the bond dissociation energy (D^0, eV) at 298 K for CO, CH_4, and at 0 K for FeO.

	BP86		PBE		TPSS		ωB97XD		Experiment*	
	r_e	D°	r_e	D°	r_e	D°	r_e	D°	r_e	D°
C—O	1.137	11.48	1.136	11.53	1.134	10.89	1.123	10.97	1.128[a]	11.16[d]
CH_3-H	1.097	4.48	1.096	4.38	1.093	4.40	1.089	4.43	1.087[b]	4.55[d]
Fe—O	1.603	5.34	1.603	5.37	1.603	4.97	1.599	4.27	1.616[c]	4.18[e]

* See Ref.: (a) [24], (b) [25], (c)[26], (d) [27], (e) [28].

FeO. The TPSS shows a similar performance to ωB97XD whereas the D° value of FeO is not very well calculated.

Although chemically very simple, Fe_2O_3 single cluster could adopt different configurations depending on its point group and spin state. Fig. 1 plot the lowest energy structures of Fe_2O_3 of the same C_{2v} point group with different conformers and spin multiplicities. The ωB97XD/def2tzvp predicts that Fe_2O_3 has a nonet ground state, ($^9B_2$, C_{2v} point group) which is greatly lower in energy (by 1.95 eV) than the low-spin septet Fe_2O_3 (^{7}C4). The ground state of Fe_2O_3 ($^9B_2$) is composed of a four-membered ring (—Fe—O—Fe—O—) and one terminal Fe—O bond.

Fig. 2 reveals plot of the DFT calculated reaction pathways for CO oxidation by Fe_2O_3, Fe_2O_2, and Fe_2O respectively. The corresponded geometries and energies of the optimized structures are listed as Table S1 (see Supporting Information). DFT investigation shows that the reactions are all subject to relatively low overall reaction barriers (ORBs). ORB is defined relative to the separated CO and the individual iron oxides: 0.25 eV (Fe_2O_3), −0.02 eV (Fe_2O_2), 0.12 eV (Fe_2O). In contrast to Fe_2O_2, and Fe_2O, in the reaction of CO with the Fe_2O_3, CO is easily oxidized by Fe—O terminal bond. In this case, the absolute reaction barrier (ARB, defined as the energy difference between the transition state (TS) and the corresponded intermediate (I)) is the lowest, 0.23 eV. Subsequent reduction of Fe_2O_3 by CO is much favorable since ORBs are lower. In Fig. 2, although the ωB97XD/def2tzvp predicts that overall reactions of Fe_2O_2, and Fe_2O reduction are exothermic, CO prefers to stay adsorbed in the first intermediate state ^{9}I1/B/ and ^{9}I1/C/ respectively since the corresponded ARBs are high: 1.55 eV (Fe_2O_2), 1.54 eV (Fe_2O). The ORBs values of the Fe_2O_{1-3} + CO systems suggest that the Fe—O bond activation barriers are higher for an iron center connected to the three oxygens (as in Fe_2O_3) than for the iron center connected to the less oxygens (as Fe_2O_2 and Fe_2O). DFT calculations point out that the Fe—O bond activation is the rate-limiting step for the subsequent C=O bond formation and CO_2 molecule subtraction.

We have checked the competing mechanisms of Fe_2O_3 reduction by H_2 in the atmosphere of CH_4. Since under the high temperature methane easily decomposes, according to the reaction: $CH_4 \rightleftharpoons C + 2H_2$, we suggest that hydrogen is also oxidized by Fe_2O_3. The reaction pathways shown in Figs. 3 and 4 predict that the reduction of Fe_2O_3, by H_2 goes faster than by CH_4, (0.81 eV vs 1.2 eV). The negative ORB is observed for $Fe_2O_2 + H_2$ (Fig. 3, path B). The only negative ORB means that reaction of Fe_2O_3 reduction by H_2 in the atmosphere of CH_4 would proceed much slower comparing to CO reduction, hence oxy-iron catalyst would reduce less. Significant ORBs for Fe_2O_3 reduction by CH_4 (Fig. 4, path A) indicate that CH_4 dissociation is rate-limiting step in processes of methane conversion by oxy-iron catalysts. The DFT calculation predicts that CH_4 preferably makes Fe—C bond which leads to the carburization of iron active site (Fig. 4, path C). The overall reaction is exothermic (−0.27 eV) and ARBs (Fig. 4, TS5/C) are lower than for the carbon oxidation by the surface oxygen to produce CO (Fig. 4, TS5/B). During CH_4 conversion the activation barrier is the highest for the CO production (ARB = 0.44 eV, ^{9}TS5/B). The more favorable process is H_2O formation via the H atom oxidation by the surface oxygen (ARB = 0.14 eV, ^{9}TS5/C). The corresponded geometries and energies of the optimized structures are listed as Tables S2-3 (see Supporting Information).

Carburization of iron active sites in atmosphere of pure methane is quite expected, since there is no other oxidizing agent to oxidize the Fe—C bond. The side-reaction of carbide formation could happen during the Fe_2O_3 reduction in the CO atmosphere as well. Under the high temperature CO easily decomposes, according to the reaction $2CO \rightleftharpoons C + CO_2$, ($\Delta H^o_{1123K} = -169.4$kJ/mol). Carbon interacts with oxygen-unsaturated iron sites without barrier to form Fe_3C: 3Fe ($^{11}A_1$, D_{3h}) + C (^{3}S) → Fe_3C ($^{11}A_1$, C_{3v}). The ωB97XD/def2tzvp calculation predicts that the high-spin conformation of Fe_3C has the lowest energy in the ground state ($^{11}A_1$, C_{3v} point group). Gibbs free energy change for adsorption of carbon on iron sites is highly negative (ΔG_{DFT} = −5.75 eV).

In contrast to the experimental conditions of OIC reduction by CH_4 in atmosphere of CO the additional oxidizing agents (as CO_2 molecules) could be present. CO_2 facilitates the oxidation of carbides and decreases the level of carburization of iron active sites.

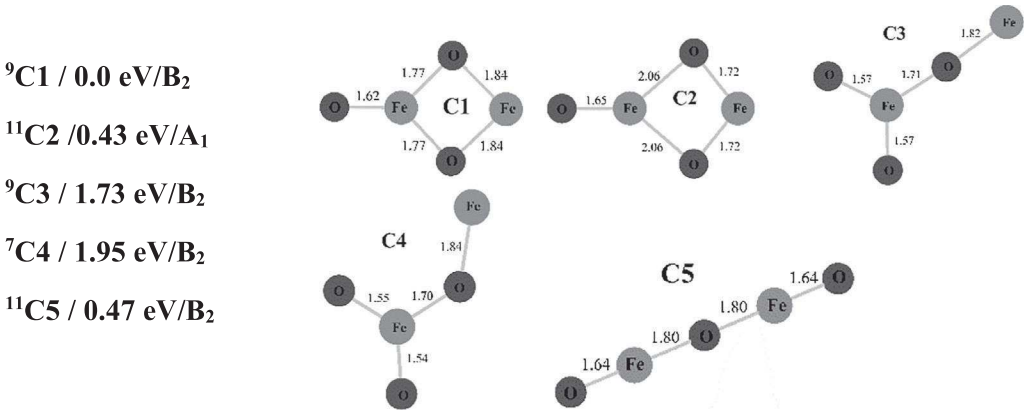

Fig. 1. ωB97XD/def2tzvp optimized structures and relative energies (zero-point vibrational energy corrected) of Fe_2O_3 cluster. The bond lengths in 0.1 nm are given. The superscripts indicate spin multiplicities and C1—C5 denote five conformers within the same C_{2v} point group.

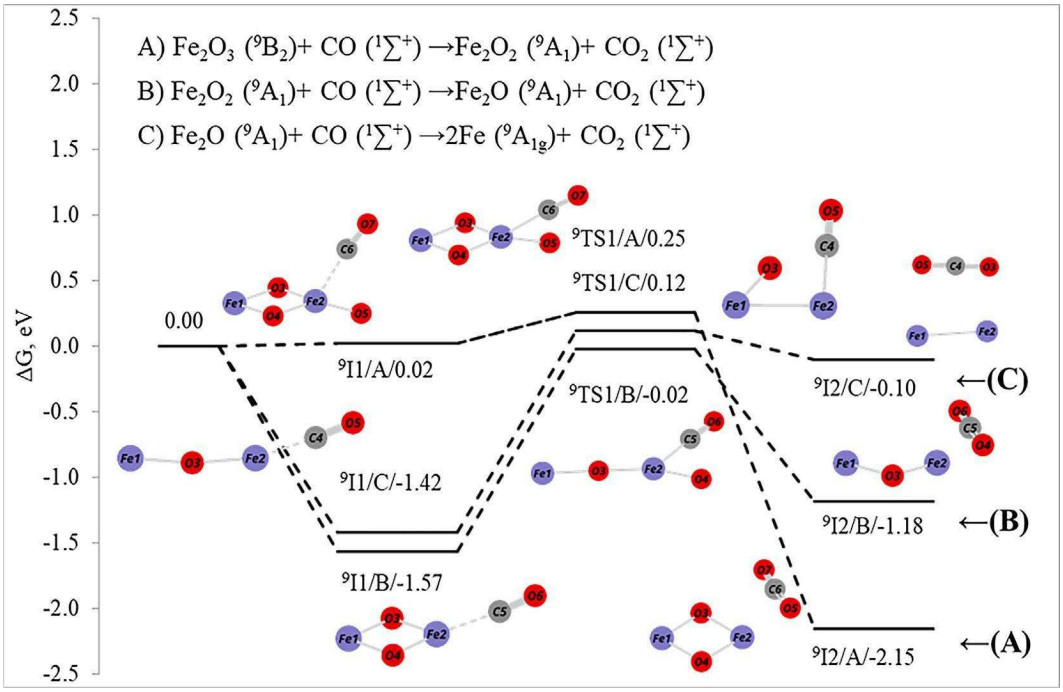

Fig. 2. ωB97XD/def2tzvp calculated reaction pathways (A–C) for Fe_2O_{1-3} + CO → Fe_2O_{0-2} + CO_2. The reaction intermediates (In), transition states (TSn), pathways (A–C) and their relative Gibbs free energies (in eV) at 298 K are given as In/A–C/ΔG or TSn/A–C/ΔG. The superscripts indicate the spin multiplicities of the systems. All of the energies are relative to the total free energy of the corresponded reagents Fe_2O_{1-3} (^{9}C1) + CO ($^1\Sigma^+$).

Fig. 5 displays the DFT calculated reaction pathway for Fe_3C oxidation by CO_2. The corresponded geometries and energies of the optimized structures are listed as Table S4 (see Supporting Information). Negative ORB of −0.09 eV is determined for the reaction. The second negative ARB for the $Fe_3C + CO_2$ system (^{11}TS2) suggests the fast oxidation of Fe_3C in presence of CO_2. Thus, the DFT reveals mechanisms to explain why XRD [3] have shown that none of Fe_3C was produced from CO reduction of the fresh oxy-iron catalysts. Meanwhile in atmosphere of CH_4 catalysts reduced significantly less and with formation of Fe_3C. This agreement between theory and experiment enables us to draw qualitative conclusions concerning the mechanisms of CO and CH_4 oxidation on Fe_xO_y clusters based on the DFT calculations.

4. Discussion

The processes of CO oxidation on different iron oxide clusters are very similar, even though the relative energies of the reaction intermediates and transition states depend on level of iron saturation by oxygen in the individual clusters. We can summarize, that two main steps are present in the oxidation of CO by Fe_2O_{1-3} clusters: (1) the intermediates formation that involves carbon-iron interaction and (2) the Fe—O bond activation that in most cases determines the ORB. Iron center should be opened for the initial intermediate (Fe_xO_y-CO/I1) formation. For an oxygen-saturated iron site the CO has less chance to approach iron. Thus, the CO displays a weaker interaction with an oxygen-saturated iron center (modeled by Fe_2O_3) than with an oxygen-unsaturated iron center (modeled by Fe_2O). We performed the second order perturbation theory analysis of the Fock matrix in NBO basis to check the character of the carbon-iron interaction in the initial intermediates We assume that the larger the perturbation energy value ($E^{(2)}$), the more intensive is the interaction between electron donors and the greater the extent of conjugation of the whole system. Delocalization of electron density between occupied Lewis type (bond or lone pair) NBO orbitals and formally unoccupied (antibonding) non Lewis NBO orbital's correspond to a stabling donor-acceptor interaction In Table 2 we provide only $E^{(2)}$ values of donor-acceptor for Fe—C and Fe—CO interactions. More data is given in Table S5 in the Supporting Information. The analysis presented in Tables 2 revealed that in Fe_2O_{1-3}-CO structures the orbital overlap between σ (Fe—C) and σ* (Fe—C) anti-bond orbital has less than 0.25 kcal/mol and hence gives no stabilization to the structures of first intermediates. The electron donations are observed from NBO of Fe to π*(C—O) which stabilize ^{9}I1/A, ^{9}I1/B and ^{9}I1/C structures by 0.32, 9.85 and 42.57 kcal/mol, respectively. This is in line with changes of their Gibbs free energy of formation (Fig. 2) and our previous statement that oxygen-saturated iron center in Fe_2O_3 has the weakest interaction with CO.

The natural bond orbitals of Fe—C interactions are displayed below and reveal that there exist two types of bonding between iron and carbon of CO: σ-bond is formed by both α- and β-spin orbitals and π-bond is formed by β-spin orbitals. In general, in all studied Fe_2O_{1-3}-CO clusters σ(Fe—C) bond is formed from $sp^{0.5}$ hybrid on carbon (which is the mixture of ∼65% *s*, ∼35% *p* AO) and gives less than 0.25 kcal/mol stabilization to the intermediate structures. It is interesting to note, that π(Fe—C) bond was found just in Fe_2O_2 + CO interacting system. It could be explained by the bonds conjugation in the ring structure of Fe_2O_2-CO. π(Fe—C) bond is formed from $sp^{3.83}d^{5.77}$ hybrid on iron, which is the mixture of 9% *s*, 36% *p*, and 54% *d* AO and gives high stabilization of 16.98 kcal/mol to the ^{9}I1/B structure (Table 2).

Fe_2O_{1-3} + CO, (Fig. 2):

^{9}I1/A: $\sigma_{FeC} = 0.942(sp^{0.51})_C + 0.337(sp^{2.88}d^{0.23})_{Fe}$
max AO[%]: s(66%)p(34%)
^{9}I1/B: $\sigma_{FeC} = 0.921(sp^{0.51})_C + 0.389(sp^{1.55}d^{0.03})_{Fe}$
max AO[%]: s(66%)p(34%)
$\pi_{FeC} = 0.839(sp^{3.83}d^{5.77})_{Fe} + 0.544(p)_C$
max AO[%]: s(9%)p(36%)d(54%)
^{9}I1/C: $\sigma_{FeC} = 0.911(sp^{0.54})_C + 0.413(sp^{0.35}d^{0.11})_{Fe}$
max AO[%]: s(65%)p(35%)

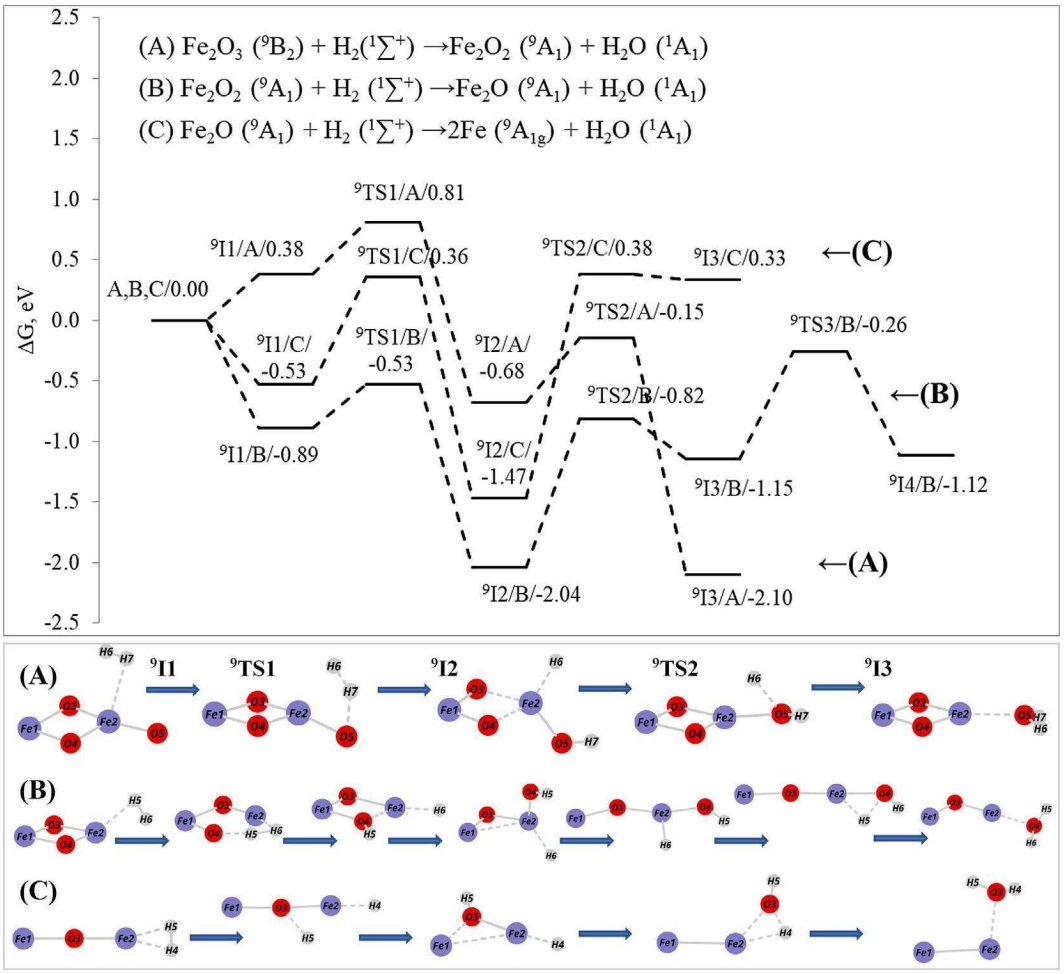

Fig. 3. ωB97XD/def2tzvp calculated reaction pathways (A–C) for $Fe_2O_{1-3} + H_2 \rightarrow Fe_2O_{0-2} + H_2O$. See caption of Fig. 2 for explanations. The potential profiles and geometries are given for spin multiplicity 9. All of the energies are relative to the total free energy of the corresponded reagents Fe_2O_{1-3} ($^9B_2$) + H_2 ($^1\Sigma^+$).

After the initial intermediate formation, the second critical step involves terminal Fe—O bond activation. As could be seen from Fig. 2 the Fe—O activation barriers also depend on the level of oxygen saturation of iron. The ARB is higher for the Fe—O activation in Fe_2O_3, than in Fe_2O (0.25 eV vs 0.12 eV). Following Fe—O bond activation, the reaction is driven by new C=O bond formation which is facile due to favorable thermodynamics: CO_2 (O—CO) bond enthalpy at 298 K is 5.54 eV, whereas those of Fe_2O_3 ($^9B_2$) → Fe_2O_2 ($^9A_1$) + O(^{3}P) is 4.03 eV based on ωB97XD/def2tzvp calculations.

The process of CH_4 conversion on Fe_2O_3 cluster is more complicated and follows different pathways. The main steps, which are present: CH_4 dissociation, Fe—C and O—H interactions, and Fe—O bonds activation. The first step in these transformations involves CH_4 adsorption onto the Fe_2O_3 cluster (Fig. 4). The NBO analysis reveals that there is no direct Fe—C interaction at this point. The Fe_2O_3—CH_4 structure is weakly stabilized by the orbital overlap between σ (C—H) and NBO of Fe, while the strongest stabilization is provided by electron donations from lone pairs of oxygens to the Fe NBO (Table S5). The weak Fe—C interaction appeared after CH_4 dissociation due to orbital overlap between σ (Fe3—C6) and σ* (Fe3—C6) anti-bond orbital. σ(Fe—C) is formed from $sp^{4.31}$ hybrid on carbon (which is the mixture of 19% s, 81% p AO) and gives 1.76 kcal/mol stabilization to the second intermediate structure ^{9}I2/A (Table 2). The stronger stabilization (19.71 and 12.74 kcal/mol) is provided by electron donations from O4 and O5 to σ* (Fe3—C6), respectively (Table S5).

Fe_2O_3 + CH_4, (Fig. 4):

^{9}I2/A: $\sigma_{FeC} = 0.812(sp^{4.31})_C + 0.584(sp^{0.52}d^{1.86})_{Fe}$
max AO[%]: s(19%)p(81%)

The second critical step of the Fe_2O_3 + CH_4 reaction involves C—H bonds activation for further CH_4 dissociation. We found that the subsequential dissociations of CH_4 are the rate-determining processes and the third dissociation step is found to be the dominant rate-limiting-step with the highest ORB of 1.39 eV (Fig. 4. ^{9}TS3/A). The subtraction of H_2O is more favorable than complete CH_4 dissociation (ORBs: 0.43 eV vs 1.39 eV), so reaction would proceed through the path B (Fig. 4). The subsequent C or H oxidation by the oxygens of Fe_2O_3 goes through the Fe—O bond activation. The activation barriers for H_2O formation is around 0.14 eV, meanwhile the interaction between C and O for desorption of CO is identified to be one more rate-limiting-step with ARB of 0.44 eV. In light of high ARBs of C—O formation and the low ARBs of Fe—C formation the preferable deposition of carbon (carburization) on the active iron sites is predicted by DFT calculations. The same formation of iron carbides has been shown for reaction of Fe_2O_3 + CO, however the presence of oxidizer CO_2 in the atmosphere of CO easily decomposes Fe_3C with negative ORB of −0.09 eV (Fig. 5). For the Fe_2O_3 + CH_4 interaction, the competing processes of Fe_2O_3 reduction by hydrogen is found to have lower ORB, compare to the reduction by CH_4 (0.8 eV vs 1.39 eV). The reduction of Fe_2O_{1-3} clusters by H_2 removes oxygens from catalyst, thus 1) decreases

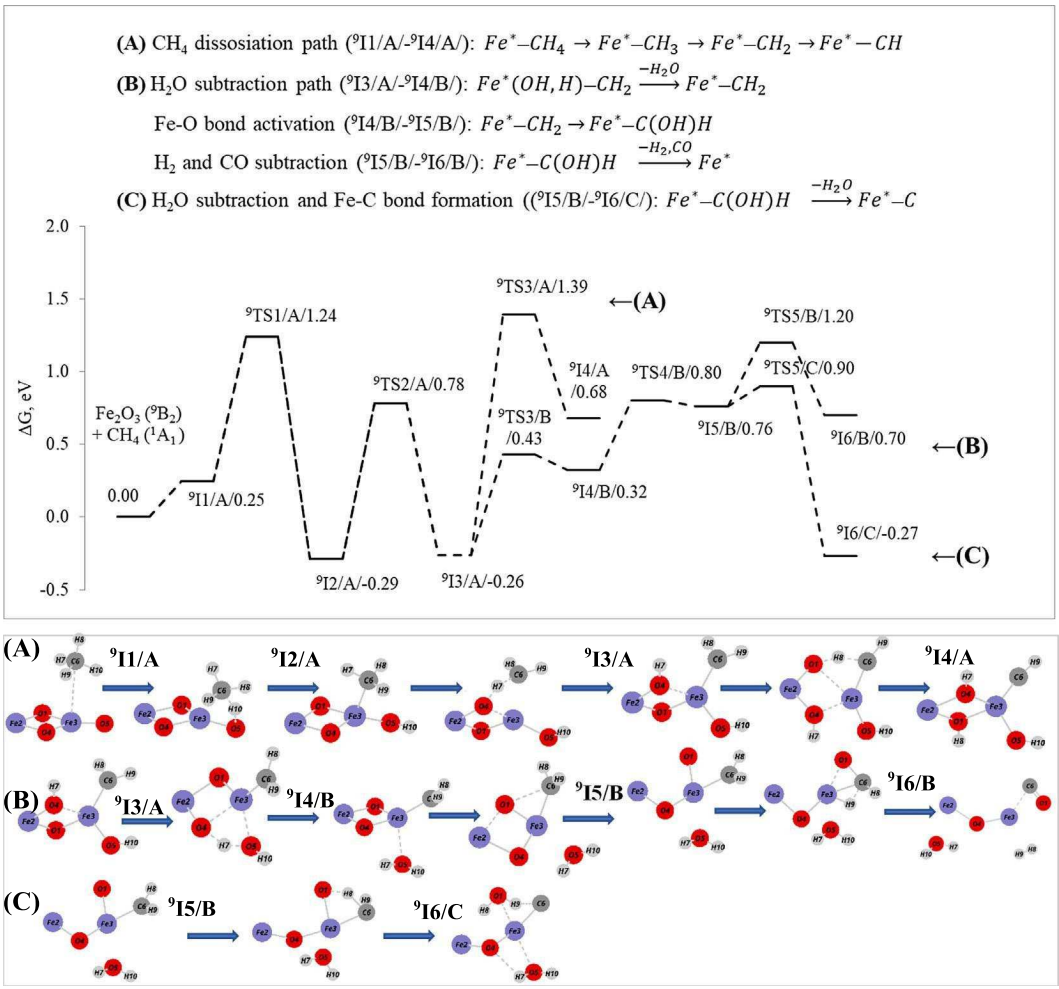

Fig. 4. ωB97XD/def2tzvp calculated reaction pathways (A, B) for Fe_2O_3 + CH_4. See caption of Fig. 2 for explanations. The potential profiles and geometries are given for spin multiplicity 9. All of the energies are relative to the total free energy of the corresponded reagents Fe_2O_3 ($^9B_2$) + CH_4 ($^1A_1$).

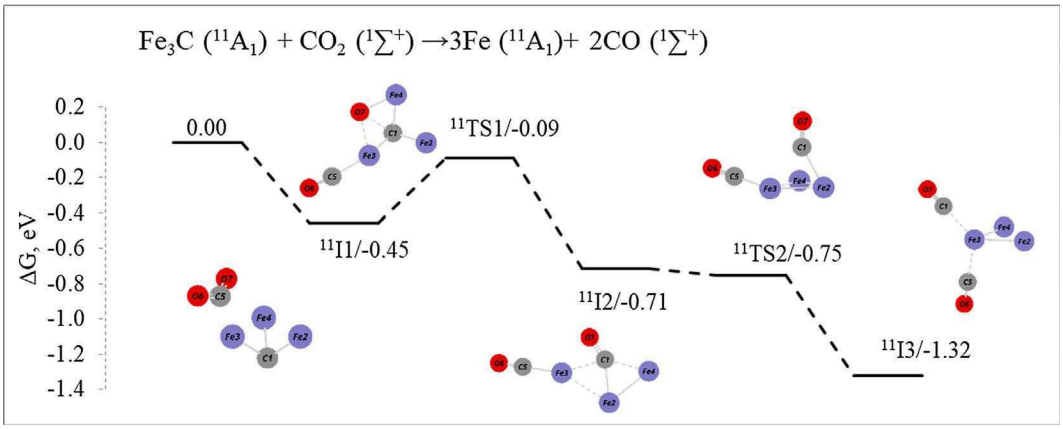

Fig. 5. ωB97XD/def2tzvp calculated reaction pathway for Fe_3C ($^{11}A_1$) + CO_2 ($^1\sum^+$) →3Fe ($^{11}A_1$) + 2CO ($^1\sum^+$). See caption of Fig. 2 for explanations. The potential profiles and geometries are given for spin multiplicity 11. All of the energies are relative to the total free energy of the corresponded reagents Fe_3C ($^{11}A_1$) + CO_2 ($^1\sum^+$).

the overall level of CO production, and 2) increases level of carburization of iron sites.

Presented here first-principle DFT calculations are in agreement with experimental data of Fan and co-workers [3.13] such as the (1) better CaO–Fe_xO_y reduction in atmosphere of CO compared to CH_4, and (2) observed iron carbides formation for CH_4 chemical looping process and the absence of Fe_3C after the reduced oxy-iron catalyst by CO. Thus, it was shown that gas-phase investigations of reactions of small Fe_2O_{1-3} clusters with gas molecules provide an applicable theoretical model for the studying of the intrinsic mechanisms of CO and CH_4 conversions on active iron sites of OIC. The presented DFT results are reliable enough to describe the side-effects of carburization during the CLHG process.

Table 2
Second order perturbation theory analysis of the Fock matrix in NBO basis in first intermediates (^{9}I1) in Fe_2O_{1-3} + CO and Fe_2O_3 + CH_4 reactions.

Intermediate[a]	Donor (i)	NBO Type	Occ. *e*	Acceptor (j)	NBO Type	Occ. *e*	$E^{(2)}$[b], kcal/mol
$Fe_2O_{0,3}$ + CO							
Fig. 2, ^{9}I1/A	Fe2—C6	σ	0.98	Fe2—C6	σ*	0.05	<0.25
	Fe2	LP(3)	0.99	C6—O7	π*	0.05	0.32
Fig. 2, ^{9}I1/B	Fe2—C5	σ	0.99	Fe2—C5	σ*	0.01	<0.25
	Fe2—C5	π	0.71	Fe2—C5	π*	0.19	16.98
	Fe2	LP(5)	0.95	C5—O6	π*	0.03	9.85
Fig. 2, ^{9}I1/C	Fe2—C4	σ	0.99	Fe2—C4	σ*	0.04	<0.25
	Fe2	LP(2)	0.81	C5—O5	π*	0.18	42.57
Fe_2O_3 + CH_4							
Fig. 4, ^{9}I2/A	Fe3—C6	σ	0.98	Fe3—C6	σ*	0.04	1.76

[a] Fig. 2: ^{9}I1/A - Fe_2O_3 + CO; ^{9}I1/B - Fe_2O_2 + CO; ^{9}I1/C - Fe_2O + CO. Fig. 4: ^{9}I2/A - Fe_2O_3 + CH_4.
[b] $E^{(2)}$ means energy of hyper conjugative interaction (stabilization energy).

5. Summary

The first-principle DFT calculations are applied for investigation of the reactivity of iron-oxide based catalysts toward CO and CH_4. Reducing agent-dependent reactivity is observed and well interpreted by the DFT calculations. Two necessary steps in the oxidation of CO by Fe_2O_{1-3} clusters have been revealed: (1) the initial intermediate formation that involves Fe—CO interaction and (2) the Fe—O bond activation that in most cases determines the overall reaction barrier. The Fe—O bond activation energy varies from −0.02 (Fe_2O) to 0.25 eV (Fe_2O_3) and depends on the level of iron saturation by the oxygens. The processes of CH_4 oxidation by Fe_2O_3 goes through the Fe—O bond activation for the subsequent CO or H_2O formation. It was shown, that the dissociation of CH_4 is the dominant rate-determining process, and the third dissociation step is found to be the rate-limiting-step with activation barrier of 1.39 eV. This result is in agreement with periodic DFT calculations[11]. The competing processes of Fe_2O_{1-3} reduction by H_2 in atmosphere of CH_4 is proposed and studied by DFT calculations. The dissociation of H_2 is found to be the rate-limiting-step for the competing reduction mechanism with minimum activation energy 0.81 eV. The overall reaction barrier for Fe_2O_3 reduction by H_2 is lower than for CH_4 by 0.58 eV. DFT calculations predict that Fe_3C forms with no barrier through the reaction between carbon and completely reduced iron active sites: 3Fe ($^{11}A_1$. D_{3h}) + C (^3S) → Fe_3C ($^{11}A_1$. C_{3v}), ΔG_{DFT} =−5.75 eV. Meanwhile, Fe_3C does not decompose in atmosphere of CH_4 due to the absence of oxidizing agents. In contrast, atmosphere of CO facilitates Fe_3C decomposition to Fe due to presence of CO_2. The findings revealed here for the gas-phase reactions can be used to prevent side-reactions of carburization in related CO and CH_4 chemical looping process over the oxy-iron based catalysts at a molecular level.

Acknowledgments

This work was supported by NSF EPSCoR RII Grant No. OIA-1632899. We thank the Mississippi Center for Supercomputer Research (Oxford. MS. USA) for an allotment of computer time. The authors acknowledge the Extreme Science and Engineering Discovery Environment (XSEDE) award DMR100088 which is supported by National Science Foundation Grant Number ACI-1053575.

References

[1] R.A. van Santen, M. Neurock, Molecular Heterogeneous Catalysis, Wiley-VCH, 2006.
[2] Organometallic Oxidation Catalysis, vol. 22, Springer Berlin Heidelberg, 2007.
[3] Z. Sun et al., $Ca_2Fe_2O_5$: a promising oxygen carrier for CO/CH_4 conversion and almost-pure H_2 production with inherent CO_2 capture over a two-step chemical looping hydrogen generation process, Appl. Energy 211 (2018) 431–442.
[4] M. Ismail, W. Liu, S.A. Scott, The performance of Fe_2O_3-CaO oxygen carriers and the interaction of iron oxides with CaO during chemical looping combustion and H_2 production, Energy Proc. 63 (2014) 87–97.
[5] R.C. Ropp, The alkaline earths as metals, in: Encyclopedia of the Alkaline Earth Compounds, Elsevier, 2013, pp. 1–23, https://doi.org/10.1016/B978-0-444-59550-8.00001-6.
[6] A.T. Bell, The impact of nanoscience on heterogeneous catalysis, Science (80-) 299 (2003) 1688–1691.
[7] P. Jena, A.W. Castleman, Clusters: a bridge across the disciplines of physics and chemistry, Proc. Natl. Acad. Sci. 103 (2006) 10560–10569.
[8] P. Li, D.E. Miser, S. Rabiei, R.T. Yadav, M.R. Hajaligol, The removal of carbon monoxide by iron oxide nanoparticles, Appl. Catal. B Environ. 43 (2003) 151–162.
[9] Y. Zheng et al., Quasicubic α-Fe_2O_3 nanoparticles with excellent catalytic performance, J. Phys. Chem. B 110 (2006) 3093–3097.
[10] W. Xue, Z.-C. Wang, S.-G. He, Y. Xie, E.R. Bernstein, Experimental and theoretical study of the reactions between small neutral iron oxide clusters and carbon monoxide, J. Am. Chem. Soc. 130 (2008) 15879–15888.
[11] L. Huang, M. Tang, M. Fan, H. Cheng, Density functional theory study on the reaction between hematite and methane during chemical looping process, Appl. Energy 159 (2015) 132–144.
[12] B.V. Reddy, S.N. Khanna, Self-stimulated NO reduction and CO oxidation by iron oxide clusters, Phys. Rev. Lett. 93 (2004) 068301.
[13] Z. Sun et al., Improvement of H_2-rich gas production with tar abatement from pine wood conversion over bi-functional $Ca_2Fe_2O_5$ catalyst: investigation of inner-looping redox reaction and promoting mechanisms, Appl. Energy 212 (2018) 931–943.
[14] M.J. Frisch et al., Gaussian 09, Revision D.01, Gaussian, Inc., Wallingford, CT, 2009.
[15] H. Hirao, D. Kumar, L. Que, S. Shaik, Two-state reactivity in alkane hydroxylation by non-heme iron−oxo complexes, J. Am. Chem. Soc. 128 (2006) 8590–8606.
[16] H.B. Schlegel, Optimization of equilibrium geometries and transition structures, J. Comput. Chem. 3 (1982) 214–218.
[17] C. Peng, P.Y. Ayala, H.B. Schlegel, M.J. Frisch, Using redundant internal coordinates to optimize equilibrium geometries and transition states, J. Comput. Chem. 17 (1996) 49–56.
[18] J.-D. Chai, M. Head-Gordon, Long-range corrected hybrid density functionals with damped atom–atom dispersion corrections, Phys. Chem. Chem. Phys. 10 (2008) 6615.
[19] F. Weigend, R. Ahlrichs, Balanced basis sets of split valence, triple zeta valence and quadruple zeta valence quality for H to Rn: design and assessment of accuracy, Phys. Chem. Chem. Phys. 7 (2005) 3297.
[20] S. Dohm, A. Hansen, M. Steinmetz, S. Grimme, M.P. Checinski, Comprehensive thermochemical benchmark set of realistic closed-shell metal organic reactions, J. Chem. Theory Comput. (2018), https://doi.org/10.1021/acs.jctc.7b01183.
[21] J.P. Perdew, Density-functional approximation for the correlation energy of the inhomogeneous electron gas, Phys. Rev. B 33 (1986) 8822–8824.
[22] J.P. Perdew, K. Burke, M. Ernzerhof, Generalized gradient approximation made simple, Phys. Rev. Lett. 77 (1996) 3865–3868.
[23] J. Tao, J.P. Perdew, V.N. Staroverov, G.E. Scuseria, Climbing the density functional ladder: nonempirical meta-generalized gradient approximation designed for molecules and solids, Phys. Rev. Lett. 91 (2003) 146401.
[24] A.F. Wells, Structural Inorganic Chemistry, fourth ed., Clarendon press, 1975.
[25] G.B. Ellison, P.C. Engelking, W.C. Lineberger, An experimental determination of the geometry and electron affinity of methyl radical, J. Am. Chem. Soc. 100 (1978) 2556–2558.
[26] A.-C. Cheung, N. Lee, A. Lyyra, A. Merer, A. Taylor, Spectroscopic properties of the 5Δi ground state of FeO, J. Mol. Spectrosc. 95 (1982) 213–225.
[27] B. deB. Darwent, Bond dissociation energies in simple molecules, Nat. Stand. Ref. Data Ser., Nat. Bur. Stand. (US), 1970.
[28] D.A. Chestakov, D.H. Parker, A.V. Baklanov, Iron monoxide photodissociation, J. Chem. Phys. 122 (2005) 084302.